Nucleon Structure Studies with Electromagnetic Probes

Michael F. Vineyard
Department of Physics and Astronomy, Union College, Schenectady, NY 12308
Period: March 1, 2008 - June 14, 2009
Contract Number: DE-FG02-03ER41252

1 Introduction

Summarized in this report is the progress achieved during the period from March 1, 2008 to June 14, 2009 under contract number DE-FG02-03ER41252. This is the final technical report under this contract. The experimental work described here is part of the electromagnetic nuclear physics program of the CEBAF Large Acceptance Spectrometer (CLAS) Collaboration at the Thomas Jefferson National Accelerator Facility (Jefferson Lab) that published 17 journal articles during the period of this report [1, 2, 3, 4, 5, 6, 7, 8, 9, 10, 11, 12, 13, 14, 15, 16, 17]. One of these journal articles reported on the results of precise measurements of the neutron magnetic form factor [14]. I was a spokesperson on this experiment [18] and the publication of these results is the culmination of years of effort by a small subset of the CLAS Collaboration. As usual, undergraduate students were involved in all aspects of this work. Three Union College students participated in this program during the window of this report and one presented a paper on his work at the 2009 National Conference on Undergraduate Research (NCUR22) [19].

In this report, I discuss recent progress on the measurements of the neutron magnetic form factor and describe my service work for the CLAS Collaboration.

2 Measurements of the Neutron Magnetic Form Factor

The elastic electromagnetic form factors of the proton and neutron are fundamental quantities related to their spatial charge and current distributions. The dominant features of the larger form factors G_M^p, G_E^p, and G_M^n were established in the 1960's: the dipole form $G_D = (1+Q^2/\Lambda)^{-2}$ where $\Lambda = 0.71$ GeV^2 gave a good description of these form factors ($G_M^p/\mu_p \approx G_M^n/\mu_n \approx G_E^p \approx G_D$) within experimental uncertainties, corresponding (at least for $Q^2 \ll 1$ GeV^2 or large radii) to an exponential falloff in the spatial densities of charge and magnetization. Recent Jefferson Lab results on the proton form factors show a dramatic departure from the dipole form even at moderate Q^2 [20] while the neutron magnetic form factor G_M^n falls below the dipole form at high Q^2 ($G_M^n/\mu_n G_D = 0.62 \pm 0.15$ at $Q^2 = 10$ GeV^2 [21]). Describing all these modern results with nucleon models and lattice calculations has been a challenge [22, 23, 24, 25, 26]. Also, the elastic form factors are the zeroth moment of the generalized parton distributions (GPDs), and thus constrain GPD models [23]. Last, we note that some models predict significant deviations from the dipole for $Q2 < 5GeV^2$ [24, 25, 26].

To distinguish among different models, high precision and large Q^2 coverage are important. At larger momentum transfer G_n^M is known much more poorly than the proton form factors [27]. In this Letter we report on a new measurement of G_n^M in the range $Q^2 = 1.0 - 4.8GeV^2$ at Jefferson Lab. The precision and coverage of these results eclipse the world's data in this Q^2 range. Systematic uncertainties were held to 2.5% or less.

In the absence of a free neutron target, we measure the ratio R of the cross sections for the $^2\mathrm{H}(e,e'n)p$ and $^2\mathrm{H}(e,e'p)n$ reactions in quasielastic (QE) scattering on deuterium. A nucleon with most of the momentum from the scattered electron is detected in coincidence with the final-state electron. The ratio R is defined as $R = \frac{d\sigma}{d\Omega}[^2\mathrm{H}(e,e'n)_{QE}] / \frac{d\sigma}{d\Omega}[^2\mathrm{H}(e,e'p)_{QE}]$ [28, 29, 30, 31] and

$$R = a(E, Q^2, \theta_{pq}^{max}, W_{max}^2) \times \frac{\sigma_{Mott}\left(\frac{(G_E^n)^2+\tau(G_M^n)^2}{1+\tau} + 2\tau\tan^2\frac{\theta}{2}(G_M^n)^2\right)}{\frac{d\sigma}{d\Omega}[\mathrm{H}(e,e')p]}, \quad (1)$$

where E is the beam energy, σ_{Mott} is the cross section for scattering off a scalar (spinless), point particle of unit charge, $\tau = Q^2/4M^2$, M is the nucleon mass, and θ is the electron scattering angle. The factor $a(E, Q^2, \theta_{pq}^{max}, W_{max}^2)$ corrects for nuclear effects and depends on E and cuts on θ_{pq}^{max}, the maximum angle between the nucleon direction and the three-momentum transfer $\vec{q}$, and W_{max}^2, the square of the maximum value of the mass recoiling against the electron assuming a stationary target. We used the one-photon exchange approximation in the numerator of Eq. 1 to express the cross section in terms of the neutron form factors. The right-hand side of Eq. 1 contains the desired G_M^n along with the better-known proton cross section and the neutron electric form factor (G_E^n), which is believed to be small over the Q^2 range studied here. For QE kinematics (within a cone θ_{pq}^{max} around $\vec{q}$) G_M^n can be extracted from Eq. 1 as a function of Q^2 by relying on knowledge of the proton cross section (i.e., the Arrington parametrization [32]), G_E^n, calculations of $a(E, Q^2, \theta_{pq}^{max}, W_{max}^2)$, and measurements of R. The ratio method is less vulnerable to nuclear structure (*e.g.*, choice of deuteron wave function, *etc.*) [31] and experimental effects (*e.g.*, radiative corrections, *etc.*). The challenge here is to accurately measure the nucleon detection efficiencies.

The two reactions were measured in the CLAS detector [33] at the same time and from the same target to reduce systematic uncertainties. Two electron-beam energies were used, 2.6 GeV and 4.2 GeV. CLAS consists of six independent magnetic spectrometers each instrumented with drift chambers [34], time-of-flight (TOF) scintillators covering polar angles $8^\circ < \theta < 143^\circ$ [35], a gas-filled threshold Cherenkov counter (CC) [36], and a lead-scintillator sandwich-type electromagnetic calorimeter (EC) covering $8^\circ < \theta < 45^\circ$ [37]. CLAS was triggered on electrons by requiring a coincidence between CC and EC signals in one sector. Neutrons were measured separately in the TOF and EC. Protons were measured using the drift chambers and TOF systems. A novel dual-cell target was used consisting of two collinear cells each 5-cm long - one filled with ^{1}H and the other with ^{2}H - and separated by 4.7 cm. The downstream cell was filled with liquid hydrogen for calibrations and efficiency measurements. The upstream cell was filled with liquid deuterium for the ratio measurement. The target was made of aluminum with 20-μm aluminum windows. The CLAS vertex resolution of 2 mm enabled us to separate events from the different targets [33].

We now describe the analysis. Nucleons from quasielastic events tend to be ejected close to the direction of the 3-momentum transfer $\overrightarrow{q}$ while inelastically scattered nucleons are not [31]. We required the angle θ_{pq} between the nucleon 3-momentum $\overrightarrow{q}$ to be small ($\theta_{pq}^{max} = 2.5^\circ - 4.5^\circ$ across the Q^2 range) and integrated over all azimuthal angles about $\overrightarrow{q}$. Another cut, $W^2 < W_{max}^2 =$ 1.2 GeV^2 eliminated most inelastic events that survived the θ_{pq}^{max} cut. Our simulations of the quasielastic [28] and inelastic production [38] show the fraction of inelastic events surviving these cuts is less than 0.5% of the total. To measure R accurately, the solid angles of CLAS for the

$^2H\,(e,e'n)_{QE}$ and $^2H\,(e,e'p)_{QE}$ reactions have to be identical. The nucleon solid angles were matched by first determining event by event the nucleon momentum from the electron kinematics assuming quasielastic scattering. The expected proton and neutron trajectories in CLAS were checked to see if both trajectories would lie within the CLAS acceptance. Only the events where both nucleons were expected to strike the active area of CLAS were analyzed.

Once the event sample was selected, corrections for the detector efficiencies and other effects were applied. Neutrons were measured in two CLAS scintillator-based detectors: the EC and the TOF. The neutron detection efficiency (NDE) measurement was performed using tagged neutrons from the $^1\mathrm{H}(e,e'\pi^+)n$ reaction, where the mass of the unobserved neutron was inferred from the measured electron and pion kinematics and matched with possible hits in the neutron detector. The value of the detection efficiency can vary with time-dependent and rate-dependent quantities like photomultiplier tube gain so it was measured *simultaneously* with the primary deuterium measurement. The measured neutron detection efficiency for each sector for the TOF and for nine subsections in each EC sector were fitted with polynomials at low neutron momenta and a constant at high momenta. The EC efficiency typically reached a maximum value of $\approx$0.6 while the maximum TOF efficiency was 0:08 [28, 39]. The calibration target was also used to measure the proton detection efficiency using elastic scattering $p\,(e,e'p)$. The kinematics of the scattered electron were used to predict the location of the elastically scattered proton in CLAS and the event was searched for a proton at that location.

The calculation of the nuclear correction factor, $a(E,Q^2,\theta_{pq}^{max},W_{max}^2)$, in Eq. (1) is described in Ref. [40]. The cross section was calculated using the plane wave impulse approximation (PWIA) for $Q^2 \geq 1.0$ GeV^2, the AV18 deuteron wave function [41], and Glauber theory for final-state interactions (FSI). The correction is the ratio of the full calculation to the PWIA without FSI. The correction was averaged over the same θ_{pq} range used in the analysis and was less than 0.1% across the full Q^2 range.

In our analysis we assumed QE kinematics and ignored the Fermi motion that can knock the ejected nucleon out of the acceptance. To correct for this effect we simulated QE scattering from a fixed target nucleon and tested to see if it struck the active area of CLAS (an "expected" event). We then simulated the nucleon's internal motion (with the Hulthen distribution) and elastic scattering from this moving particle. With the target momentum known (in the simulation) we re-calculated the trajectory to see if it still struck CLAS and satisfied the θ_{pq}^{max} cut (an "actual" event). The ratio of actual to expected events is the correction factor for that nucleon. The ratio of these corrections for the neutron and the proton multiplies R. The correction to G_M^n is in the range $\approx 0.9-1.3$.

We present our results for the ratio R in Fig. 1 for the two beam energies and for $Q^2 > 1\,GeV^2$ where we have overlapping TOF and EC data. The corrections described above have been included and only statistical uncertainties are shown. For each beam energy we averaged the two neutron measurements (EC and TOF) weighted by the statistical uncertainties. Measurements of R at the same Q^2 but different beam energies are not expected to be the same because the kinematics are not the same [recall Eq. 1]. The data cover the Q^2 range with excellent statistical accuracy and with a large overlap between the two data sets.

A detailed study of each correction's contribution to the systematic uncertainty has been made [28]. Listed in Table 1 are the largest contributions to this systematic uncertainty along with the maximum (typical) value across the full Q^2 range. The largest contributions come from the parametrization of the neutron detection efficiencies for the TOF and EC systems. To estimate the uncertainty associated with the NDE measurement, the order of the polynomial and position of

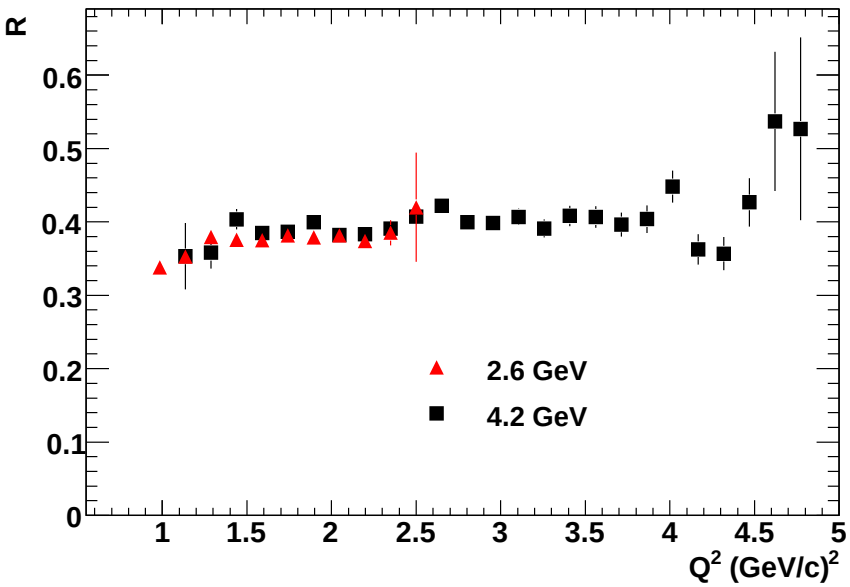

Figure 1: Results for R as a function of Q^2 for two beam energies. Each set is a weighted sum of the TOF and EC neutron measurements. Only statistical uncertainties are shown. Numerical results are reported in the CLAS Physics Data Base [39].

the edge of the constant region used to fit the data were varied to determine the effect on G_M^n as a function of Q^2. Uncertainties were in the range 0.5-3.2%.

Table 1: Upper limits (typical values) of the estimated systematic errors.

Quantity	$\delta G_M^n/G_M^n$	Quantity	$\delta G_M^n/G_M^n$
EC NDE	$<1.5\%$ (1%)	TOF NDE	$<3.2\%$ (2%)
proton σ	$<1.5\%$ (0.8%)	G_E^n	$<0.7\%$ (0.5%)
Fermi loss	$<0.9\%$ (0.5%)	θ_{pq} cut	$<1.0\%$ (0.3%)
Remainder	$<0.5\%$ (0.2%)		

The extraction of G_M^n depends on the other elastic form factors [see Eq. 1] and their uncertainties contribute to the uncertainty in G_M^n. The proton cross section uncertainty was estimated using the difference between parametrization by Arrington and Bosted [32, 42]. The average difference was <1% with a maximum of 1.5%. For G_E^n, the difference between the Galster parametrization and a fit by Lomon was used [43, 44] with a maximum uncertainty of 0.7%. The upper limit of the θ_{pq} cut was varied by $\pm$10%, changing G_M^n by a maximum of about 1.0% and by 0.3% on average [28]. The uncertainty of the Fermi motion correction was calculated using two dramatically different momentum distributions of the deuteron: a flat one and the Hulthen distribution. This correction to G_M^n changes by <1% between the two Fermi motion distributions. The quadrature sum of the remaining, maximum systematic uncertainties was less than 0.5% [28]. The final systematic uncertainty for the EC measurement was <2.4% and for the TOF measurement it was <3.6%.

The CLAS extraction of $G_M^n(Q^2)$ consists of overlapping measurements. The TOF scintillators cover the full angular range of CLAS, while the EC system covers a subset of these angles, so G_M^n

can be obtained from two independent measurements of the $e-n$ production. The experiment was performed with two beam energies with overlapping Q^2 coverage so the detection of nucleons of a given Q^2 occurs in two different regions of CLAS. Four measurements of G_M^n have been obtained from the CLAS that could have four semi-independent sets of systematic uncertainties. Shown in Fig. 2 are the results for G_M^n from the different measurements divided by $\mu_n G_D$ for normalization and to reduce the dominant Q^2 dependence. Only statistical uncertainties are shown. Here the different measurements should agree because G_M^n depends only on Q^2. The two measurements for each beam energy are consistent within the statistical uncertainties, suggesting the systematic uncertainties are well-controlled and small. The results in Fig. 2 were then combined in a weighted average as a function of Q^2. The final systematic uncertainty varied from 1.7%-2.5% across the full data range. The larger uncertainty on the parametrization of the TOF NDE (see Table 1) did not push the total, weighted uncertainty above our goal of 3%. There are considerably more calorimeter data due to its higher efficiency and the maximum EC uncertainty was 1.5% [28].

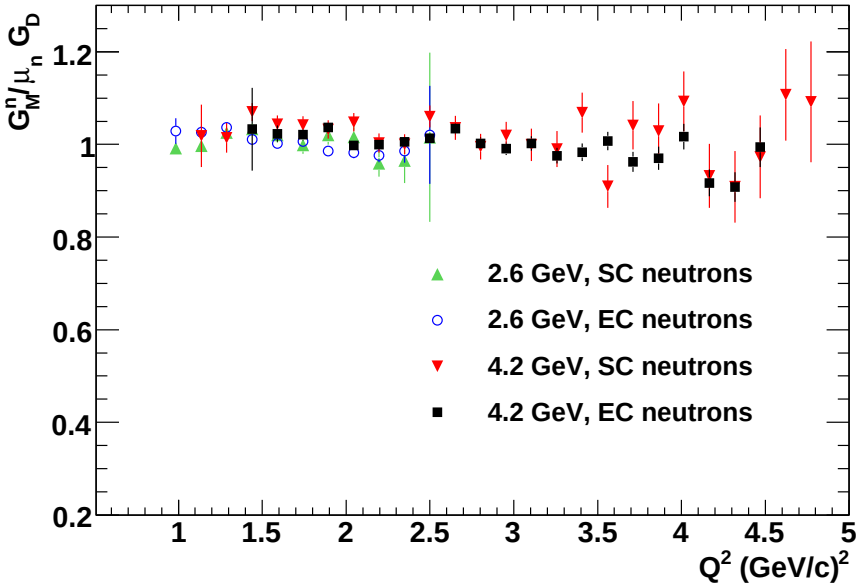

Figure 2: Results for $G_M^n/(\mu_n G_D)$ as a function of Q^2 for four different measurements (two beam energies). Only statistical uncertainties are shown.

The final, combined results for G_M^n are shown in Fig. 3 with a sample of existing data [29, 30, 45, 46, 47, 48]. The uncertainties shown are statistical only. Systematic uncertainties are represented by the band below the data. A few features are noteworthy. First, the quality and coverage of the data are dramatic improvements of the world's data set. Second, our results are consistent with that previous data, but with much smaller uncertainties. Third, the dipole form is a good representation here, which differs from parametrization and some calculations at higher Q^2 where previous results for $G_M^n/(\mu_n G_D)$ decrease with increasing Q^2 [24, 26, 27]. We note there appears to be an offset between the low-Q^2 end of our data and some earlier results [30, 45] that is about twice the uncertainty of the offset. Last, any apparent fluctuations in our results (*e.g.* at 1.29 GeV^2) are not significant enough for us to draw any firm conclusions here.

The curves shown in Fig. 3 are from Diehl *et al.* [23], Guidal *et al.* [24], and Miller *et al.* [22]

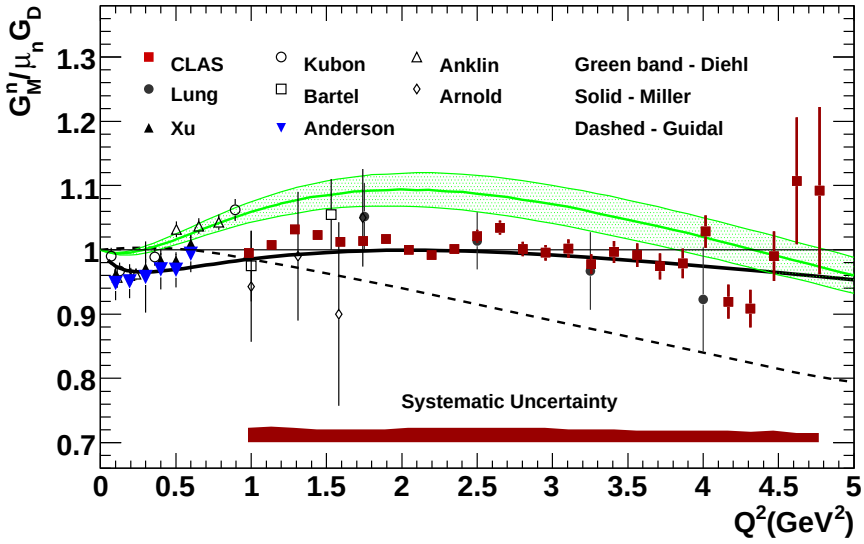

Figure 3: Results for $G_M^n/(\mu_n G_D)$ from the CLAS measurement are compared with a selection of previous data [29, 30, 45, 46, 47, 48] and theoretical calculations [22, 23, 24]. Numerical results are reported in the CLAS Physics Data Base [39].

and are all constrained by the world's previous data. In Diehl *et al.* the GPDs are parametrized and fitted to the experimental data (green band). The curve reproduces some of the low-Q^2 data, but lies above our results. Guidal *et al.* use a Regge parametrization of the GPDs to characterize the elastic nucleon form factors at low momentum transfer and extend it to higher Q^2 (dashed line). The curve reproduces the existing, higher Q^2 data (which fall well below the dipole on the range $Q^2 = 6-10\,GeV^2$), but is not consistent with our results. In Miller's calculation the nucleon is treated using light-front dynamics as a relativistic system of three bound quarks and a surrounding pion cloud (solid curve). The model achieves a good description of much of the previous nucleon form factor data even at high Q^2 and is consistent with our results.

The neutron magnetic form factor was measured in the range $Q^2 = 1.0-4.8$ GeV^2 with the CLAS detector at Jefferson Lab using the ratio of $e-n$ to $e-p$ scattering. Two incident beam energies were used and systematic uncertainties were $\leq$2.5%. Neutrons were measured with two independent systems: time-of-flight scintillators and electromagnetic calorimeters. Detector efficiencies were measured simultaneously with the production data using a dual-cell target containing ^{2}H and ^{1}H. The data provide a significant improvement in precision and coverage in this Q^2 range and are surprisingly consistent with the long-established dipole form. The calculation by Miller is in good agreement with our results.

3 CLAS Collaboration Service Work

My service to the CLAS Collaboration this year has included:

- Running 8 eight-hour shifts on experiments.

- Service on the Service Work Committee.
- Service on two analysis review committees (chair of one).
- Service on an ad hoc review committee for a journal article.
- Work on the analysis of data from G1c and G3a runs.
- Work on analysis of data from the E5 run.
- Maintenance of a Beowulf computing cluster at Union College for data analysis and simulations.
- Work on the CLAS12 Software Working Group.

References

[1] R. De Masi *et al.* (The CLAS Collaboration), Phys. Rev. C **77**, 042201(R) (2008).

[2] F.X. Girod *et al.* (The CLAS Collaboration), Phys. Rev. Lett. **100**, 162002 (2008).

[3] R. Nasseripour *et al.* (The CLAS Collaboration), Phys. Rev. C **77**, 065208 (2008).

[4] P. E. Bosted *et al.* (The CLAS Collaboration), Phys. Rev. C **78**, 015202 (2008).

[5] M. H. Wood *et al.* (The CLAS Collaboration), Phys. Rev. C **78**, 015201 (2008).

[6] J. P. Santoro *et al.* (The CLAS Collaboration), Phys. Rev. C **78**, 025210 (2008).

[7] I. G. Aznauryan *et al.* (The CLAS Collaboration), Phys. Rev. C **78**, 045209 (2008).

[8] A. S. Biselli *et al.* (The CLAS Collaboration), Phys. Rev. C **78**, 045204 (2008).

[9] G. V. Fedotov *et al.* (The CLAS Collaboration), Phys. Rev. C **79**, 015204 (2009).

[10] S. A. Morrow *et al.* (The CLAS Collaboration), Eur. Phys. J. A **39**, 5 (2009).

[11] Y. Prok *et al.* (The CLAS Collaboration), Phys. Lett. B **672**, 12-16 (2009).

[12] M. Battaglieri *et al.* (The CLAS Collaboration), Phys. Rev. Lett. **102**, 102001 (2009).

[13] M. Nozar *et al.* (The CLAS Collaboration), Phys. Rev. Lett. **102**, 102002 (2009).

[14] J. Lachniet *et al.* (The CLAS Collaboration), Phys. Rev. Lett. **102**, 192001 (2009).

[15] M. Dugger *et al.* (The CLAS Collaboration), Phys. Rev. C **79**, 065206 (2009).

[16] W. Chen *et al.* (The CLAS Collaboration), Phys. Rev. Lett. **103**, 012301 (2009).

[17] M. Osipenko *et al.* (The CLAS Collaboration), Phys. Rev. D **80**, 032004 (2009).

[18] W. K. Brooks and M. F. Vineyard (spokespersons), CEBAF Experiment Proposal E-94-017 (1994).

[19] Richard Bonventre (Michael Vineyard), "Extraction of Yields for Neutral Meson Photoproduction from the Proton and ^{3}He with the CLAS Detector at Jefferson Lab," The National Conference on Undergraduate Research (NCUR22), Salisbury University, NC, April 10-12, 2008.

[20] O. Gayou *et al.*, Phys. Lett. **88**, 092301 (2002).

[21] S. Rock *et al.*, Phys. Rev. Lett. **49**, 1139 (1982).

[22] G. A. Miller, Phys. Rev. C **66**, 032201(R) (2002).

[23] M. Diehl *et al.*, Eur. Phys. J. C **39**, 1 (2005).

[24] M. Guidal *et al.*, Phys. Rev. D **72**, 054013 (2005).

[25] M. A. Belushkin *et al.*, Phys. Rev. C **75**, 035202 (2007).

[26] J. Ashley *et al.*, Eur. Phys. J. A **19**, 9 (2004).

[27] C. Hyde-Wright and K. deJager, Annu. Rev. Nucl. Part. Sci. **54**, 217 (2004).

[28] J. D. Lachniet, Ph.D. thesis, Carnegie-Mellon University, Pittsburgh, PA, 2005.

[29] W. Bartel *et al.*, Nucl. Phys. B **58**, 429 (1973).

[30] H. Anklin *et al.*, Phys. Lett. B **428**, 248 (1998).

[31] L. Durand, Phys. Rev. **115**, 1020 (1959).

[32] J. Arrington, Phys. Rev. C **68**, 034325 (2003).

[33] B. A. Mecking *et al.*, Nucl. Instrum. Methods Phys. Res., Sect. A **503**, 513 (2003).

[34] M. Mestayer *et al.*, Nucl. Instrum. Methods Phys. Res., Sect. A **449**, 81 (2000).

[35] E. Smith *et al.*, Nucl. Instrum. Methods Phys. Res., Sect. A **432**, 265 (1999).

[36] G. Adams *et al.*, Nucl. Instrum. Methods Phys. Res., Sect. A **465**, 414 (2001).

[37] M. Amarian *et al.*, Nucl. Instrum. Methods Phys. Res., Sect. A **460**, 239 (2001).

[38] P. Corvisiero *et al.*, Nucl. Instrum. Methods Phys. Res., Sect. A **346**, 433 (1994).

[39] http://clasweb.jlab.org/physicsdb. [21]

[40] S. Jeschonnek *et al.*, Phys. Rev. C **62**, 044613 (2000). [22]

[41] R. Wiringa *et al.*, Phys. Rev. C **51**, 38 (1995). [23]

[42] P. Bosted, Phys. Rev. C **51**, 409 (1995). [24]

[43] S. Galster *et al.*, Nucl. Phys. B **32**, 221 (1971). [25]

[44] E. Lomon, Phys. Rev. C **66**, 045501 (2002). [26]

[45] G. Kubon *et al.*, Phys. Lett. B **524**, 26 (2002). [27]

[46] A. Lung *et al.*, Phys. Rev. Lett. **70**, 718 (1993). [28]

[47] B. Anderson *et al.*, Phys. Rev. C **75**, 034003 (2007). [29]

[48] R. G. Arnold *et al.*, Phys. Rev. Lett. **61**, 806 (1988).